

A continuum mechanics based four-node shell element for general non-linear analysis

Eduardo N. Dvorkin and Klaus-Jürgen Bathe

Department of Mechanical Engineering, Massachusetts Institute of Technology, Cambridge, MA 02139, USA

(Received December 1983)

ABSTRACT

A new four-node (non-flat) general quadrilateral shell element for geometric and material non-linear analysis is presented. The element is formulated using three-dimensional continuum mechanics theory and it is applicable to the analysis of thin and thick shells. The formulation of the element and the solutions to various test and demonstrative example problems are presented and discussed.

INTRODUCTION

The finite element analysis of general shell structures has been a very active field of research for a large number of years^{14,29}. However, despite the fact that many different shell elements have already been proposed, the search for a shell element capable of representing the general non-linear behaviour of shells with arbitrary geometry and loading conditions in an effective and reliable manner is still continuing very actively.

During recent years it has become apparent that two approaches for the development of shell elements are very appropriate: (1) the use of simple elements, based on the discrete-Kirchhoff approach for the analysis of thin shells^{2,5-9}; (2) the use of degenerated isoparametric elements in which fully three-dimensional stress and strain conditions are degenerated to shell behaviour^{2,3,5,7,17,19,24,29}.

The latter approach has the advantage of being independent of any particular shell theory, and this approach was used by Bathe and Bolourchi³ to formulate a general shell element for geometric and material non-linear analysis. This element has been employed very successfully when used with 9 or, in particular, 16 nodes. However, the 16-node element is quite expensive, and although it is possible to use in some analyses only a few elements to represent the total structure (see later examples) in other analyses still a fairly large number of elements need to be employed⁵.

Considering general shell analyses, much emphasis has been placed onto the development of a versatile, reliable and cost-effective 4-node shell element^{16,17,22,28}. Such element would complement the above high-order 16-node element and may be more effective in certain analyses. The difficulties in the development of such element lie in that the element should be applicable in a reliable manner to

thin and thick shells of arbitrary geometries for general non-linear analysis.

The objective in this paper is to present a simple 4-node general shell element with the following properties: the element is formulated using three-dimensional stress and strain conditions without use of a shell theory; the element is applicable to thin and thick shells and can be employed to model arbitrary geometries; the element is applicable to the conditions of large displacements and rotations but small strains, and can be used effectively in materially non-linear analysis.

The formulation of the element is quite simple and transparent, and the element has good predictive capability without containing spurious zero energy modes.

In the next section of the paper we discuss some basic considerations with respect to the assumptions used, and in the following section we present the element formulation for non-linear analysis. The results obtained in numerical solutions that demonstrate the properties of the element are given in the final section.

BASIC CONSIDERATIONS

The formulation of the 4-node shell element represents an extension of the shell element discussed previously^{2,3}, and we therefore use the same notation as in those references. Also, to focus attention onto some key issues of the formulation, we consider in this section only linear analysis conditions.

The geometry of the element (see Figure 1) is described using²:

$${}^i x_i = \sum_{k=1}^4 h_k {}^i x_i^k + \frac{r_3}{2} \sum_{k=1}^4 a_k h_k {}^i V_{ni}^k \quad (1)$$

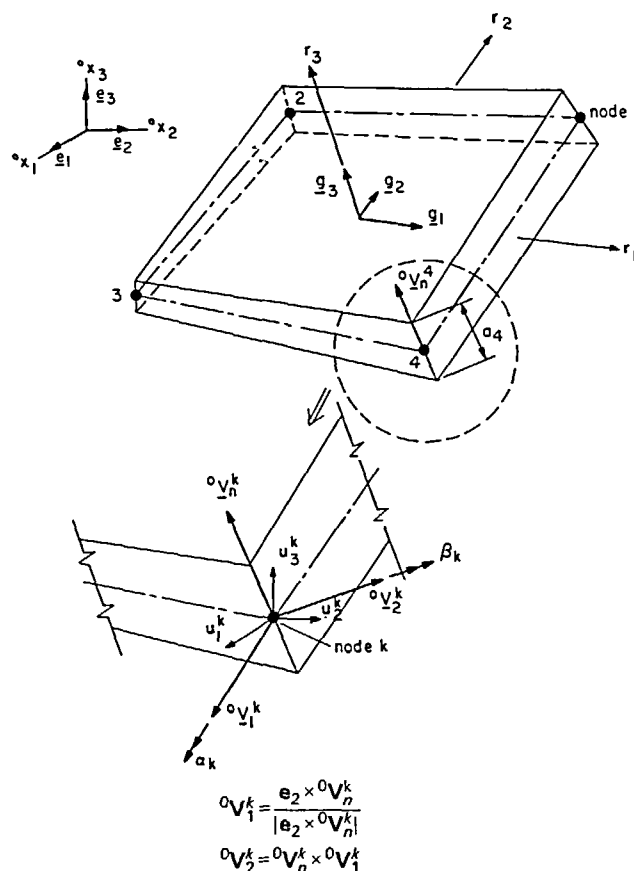


Figure 1 Four-node shell element

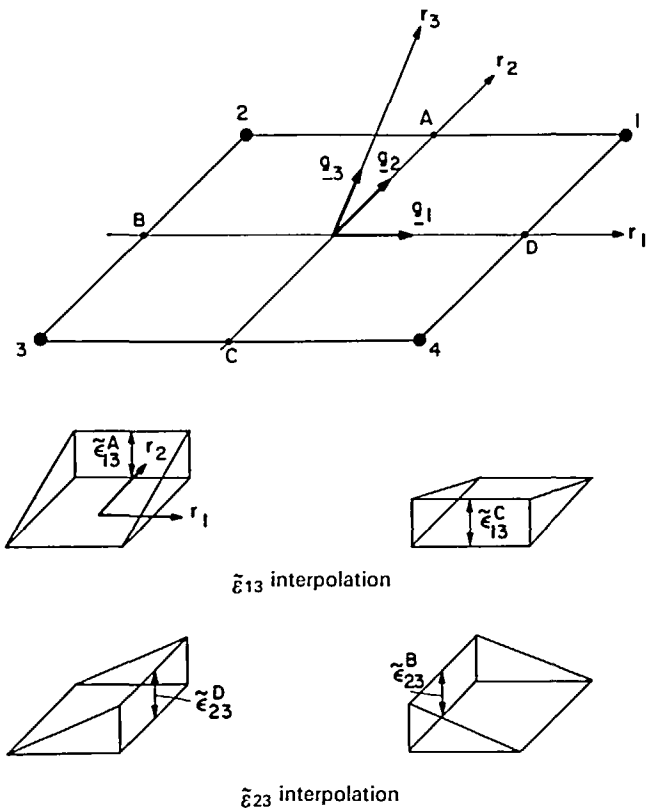


Figure 2 Interpolation functions for the transverse shear strains

where the $h_k(r_1, r_2)$ are the two-dimensional interpolation functions corresponding to node k ; the r_i are the natural coordinates; and 1x_i = Cartesian coordinates of any point in the element; ${}^1x_i^k$ = Cartesian coordinates of nodal point k ; ${}^1V_n^k$ = components of director vector at node k (which is not necessarily normal to the midsurface of the element); and a_k is the shell thickness at node k , measured along the vector ${}^1V_n^k$. The left superscript is zero for the initial geometry of the element and is equal to 1 for the deformed element geometry. Note that the thickness of the element varies and the element is in general non-flat.

The displacements of any particle with natural coordinates r_i of the shell element in the stationary Cartesian coordinate system are:

$$u_i = \sum_{k=1}^4 h_k u_i^k + \frac{r_3}{2} \sum_{k=1}^4 a_k h_k (-{}^0V_{2i}^k \alpha_k + {}^0V_{1i}^k \beta_k) \quad (2)$$

where the u_i^k are the nodal point displacements into the Cartesian coordinate directions, and the α_k and β_k are the rotations of the director vector ${}^0V_n^k$ about the ${}^0V_1^k$ and ${}^0V_2^k$ axes (see Figure 1).

A basic problem inherent in the use of the above interpolation of the displacements, and the derivation of the strain-displacement matrices therefrom, is that the element 'locks' when it is thin. This is due to the fact that with these interpolations the transverse shear strains cannot vanish at all points in the element, when it is subjected to a constant bending moment. Hence, although the basic continuum mechanics assumptions contain the Kirchhoff shell assumptions, the finite element discretization is not able to represent these assumptions rendering the element not applicable to the analysis of thin plates or shells^{2,5,7}. To solve this deficiency, various remedies based on selective and reduced integration have

been proposed^{1,7,22,23} but there is still much room for more effective and reliable elements for general non-linear analysis.

Considering our element formulation – because the problem lies in the representation of the transverse shear strains – we proceed to not evaluate these shear strains from the displacements in (2), but to introduce separate interpolations for these strain components. Since we consider non-flat shell elements, the separate interpolations are performed effectively in a convected coordinate system[†].

The choice of the interpolation for the transverse shear strain components is the key assumption in our element formulation, because adequate coupling between the element displacements and rotations must be introduced and the element should not exhibit any spurious zero energy modes. For our element we use (see Figure 2):

$$\begin{aligned} \tilde{\epsilon}_{13} &= \frac{1}{2}(1+r_2)\tilde{\epsilon}_{13}^A + \frac{1}{2}(1-r_2)\tilde{\epsilon}_{13}^C \\ \tilde{\epsilon}_{23} &= \frac{1}{2}(1+r_1)\tilde{\epsilon}_{23}^D + \frac{1}{2}(1-r_1)\tilde{\epsilon}_{23}^B \end{aligned} \quad (3)$$

Since the kinematic relations for the above shear strains are not satisfied using (3), we impose them using Lagrange multipliers^{2,27} to obtain,

$$\Pi^* = \frac{1}{2} \int_V \tilde{\tau}^{ij} \tilde{\epsilon}_{ij} dV + \int_V \lambda^{13} (\tilde{\epsilon}_{13} - \tilde{\epsilon}_{13}^{DI}) dV + \int_V \lambda^{23} (\tilde{\epsilon}_{23} - \tilde{\epsilon}_{23}^{DI}) dV - \mathcal{W} \quad (4)$$

where the $\tilde{\tau}^{ij}$ are the contravariant components of the Cauchy stress tensor^{13,15}, the $\tilde{\epsilon}_{ij}$ are the covariant components of the infinitesimal strain tensor, the λ^{13} and λ^{23} are the Lagrange multipliers, the $\tilde{\epsilon}_{13}^{DI}$ and $\tilde{\epsilon}_{23}^{DI}$ are the transverse shear strains evaluated using the displacement interpolations in (2), and \mathcal{W} is the potential of the external loads. For the Lagrange multipliers we choose the following interpolations,

$$\begin{aligned} \lambda^{13} &= \lambda^A \delta(r_1) \delta(1-r_2) + \lambda^C \delta(r_1) \delta(1+r_2) \\ \lambda^{23} &= \lambda^D \delta(r_2) \delta(1-r_1) + \lambda^B \delta(r_2) \delta(1+r_1) \end{aligned} \quad (5)$$

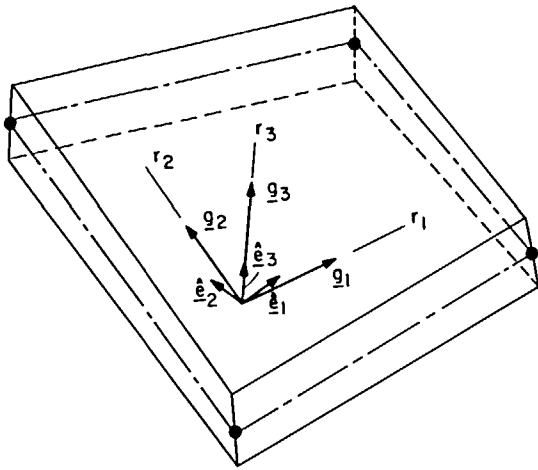
where $\delta(\dots)$ is the Dirac-delta function. This represents a weakening of the Lagrange multiplier constraint in (4)¹⁰. Substituting from (5) into (4) and invoking that $\delta\Pi^* = 0$ gives the distinct constrains:

$$\begin{aligned} \tilde{\epsilon}_{13} \Big|_{\text{at A}} &= \tilde{\epsilon}_{13}^{DI} \Big|_{\text{at A}} & \tilde{\epsilon}_{13} \Big|_{\text{at C}} &= \tilde{\epsilon}_{13}^{DI} \Big|_{\text{at C}} \\ \tilde{\epsilon}_{23} \Big|_{\text{at D}} &= \tilde{\epsilon}_{23}^{DI} \Big|_{\text{at D}} & \tilde{\epsilon}_{23} \Big|_{\text{at B}} &= \tilde{\epsilon}_{23}^{DI} \Big|_{\text{at B}} \end{aligned} \quad (6)$$

Hence, the complete element stiffness matrix is calculated using the functional:

$$\Pi^* = \frac{1}{2} \int_V \tilde{\tau}^{ij} \tilde{\epsilon}_{ij} dV - \mathcal{W} \quad (7)$$

† Note that in refs. 2 and 3, the shell element formulation is discussed in the global stationary coordinate system, because all displacement components are interpolated in the same way. To emphasize that we use here stress and strain measures in the convected coordinate system, we place a tilde (~) over these quantities.



$$\hat{e}_3 = \frac{\mathbf{g}_3}{|\mathbf{g}_3|}; \hat{e}_1 = \frac{\mathbf{g}_2 \times \hat{e}_3}{|\mathbf{g}_2 \times \hat{e}_3|}; \hat{e}_2 = \hat{e}_3 \times \hat{e}_1$$

Figure 3 Local Cartesian coordinate system used

with stress and strain components in convected coordinates and (1) and (2) to evaluate the strain components $\tilde{\epsilon}_{11}$, $\tilde{\epsilon}_{22}$ and $\tilde{\epsilon}_{12}$; (3) to evaluate the strain components $\tilde{\epsilon}_{13}$, $\tilde{\epsilon}_{23}$; and (6) to express the variables $\tilde{\epsilon}_{13}^A$, $\tilde{\epsilon}_{13}^C$, $\tilde{\epsilon}_{23}^D$, and $\tilde{\epsilon}_{23}^B$ in terms of the nodal point displacements and rotations of (2).

Considering the representation that we have chosen for the transverse shear strains, we can make the following three important observations:

(1) *The element is able to represent the six rigid body modes.* The element contains the rigid body modes because zero strains are calculated in the formulation when the element nodal point displacements and rotations correspond to an element rigid body displacement. This can be verified by using (1) to (6) to evaluate the strains, but more easily we can use the fact that the 4-node shell element of reference 3 satisfies the rigid body mode criterion. Hence, for a rigid body displacement the $\tilde{\epsilon}_{13}^{D1}$ and $\tilde{\epsilon}_{23}^{D1}$ are zero, from which it follows that also the shear strains in (3) are zero, and the rigid body mode criterion is satisfied.

(2) *The element can approximate the Kirchhoff-Love hypothesis of negligible shear deformation effects and can be used for thin shells.* Various demonstrative solutions are given in the fourth section.

(3) *Based on our studies the element does not contain any spurious zero energy modes (using a 'full' numerical integration).* We reach this observation by studying the strains along the element sides. If the element were to contain a spurious zero energy mode, the strains along every side should vanish for a displacement pattern (to be identified) other than the displacements corresponding to a true rigid body mode. However, such displacement pattern could not be identified.

Considering the practical use of the element the interpolation employed for the transverse shear strains shows that $\tilde{\epsilon}_{13}$ is constant with r_1 and in general discontinuous at $r_1 = \pm 1$ (between elements), and similarly $\tilde{\epsilon}_{23}$ is constant with r_2 and in general discontinuous at $r_2 = \pm 1$. As a consequence, the accuracy with which transverse shear stresses are predicted depends to a significant degree on the mesh used and the geometric distortions of the elements. However, our experience is

that the bending stress predictions are relatively little affected by element distortions (see examples).

To employ (7), we also need to use the appropriate constitutive relations:

$$\tilde{\tau}^{ij} = \tilde{C}^{ijkl} \tilde{\epsilon}_{kl} \quad (8)$$

where \tilde{C}^{ijkl} is the fourth-order contravariant constitutive tensor in the convected coordinates r_i . The constitutive law is known in the local Cartesian system of orthonormal base vectors \hat{e}_i , $i=1,2,3$, with the condition $\hat{e}_i \cdot \hat{e}_j = \delta_{ij}$ equal to zero², (see Figure 3). Denoting this constitutive tensor by \hat{C}^{mnop} , the constitutive tensor for (8) is obtained using the transformation:

$$\tilde{C}^{ijkl} = (\mathbf{g}^i \cdot \hat{e}_m)(\mathbf{g}^j \cdot \hat{e}_n)(\mathbf{g}^k \cdot \hat{e}_o)(\mathbf{g}^l \cdot \hat{e}_p) \hat{C}^{mnop} \quad (9)$$

where the \mathbf{g}^i are the contravariant base vectors of the convected coordinates r_i . These vectors are calculated, using the covariant base vectors \mathbf{g}_i , where:

$$\mathbf{g}_i = \frac{\partial \mathbf{x}}{\partial r_i} \quad (10)$$

with \mathbf{x} from (1) and the following relations,

$$g_{ij} = \mathbf{g}_i \cdot \mathbf{g}_j \quad (11)$$

and

$$\mathbf{g}^i = g^{ij} \mathbf{g}_j \quad (12)$$

$$g^{ij} = \frac{D^{ij}}{|\mathbf{J}|^2}$$

where D^{ij} is the cofactor of the term g_{ij} in the matrix of the metric tensor and $|\mathbf{J}|$ is the determinant of the Jacobian matrix at the point considered.

TOTAL LAGRANGIAN FORMULATION

The large displacement formulation of the shell element is based on the derivation given in ref. 2 (Section 6.3.5), and the concepts and interpolations presented in the previous section.

The geometry of the element at any time t is defined as in (1) but using the nodal point coordinates, ${}^t x_i^k$, and director vectors ${}^t \mathbf{V}_n^k$, at time t ,†

$${}^t x_i = h_k {}^t x_i^k + \frac{r_3}{2} a_k h_k {}^t V_{ni}^k \quad (13)$$

where we imply summation over k . The displacements, ${}^t u_i$, and incremental displacements, u_i , of a particle of the element at time t are hence given by:

$${}^t u_i = h_k {}^t u_i^k + \frac{r_3}{2} a_k h_k ({}^t V_{ni}^k - {}^0 V_{ni}^k) \quad (14)$$

$$u_i = h_k u_i^k + \frac{r_3}{2} a_k h_k (-{}^t V_{2i}^k \alpha_k + {}^t V_{1i}^k \beta_k)$$

where the ${}^t u_i^k$ are the nodal point displacements at time t , the u_i^k are the incremental nodal point displacements from the configuration at time t , and the variables ${}^t V_{2i}^k$, ${}^t V_{1i}^k$, α_k and β_k are defined as in (2) but referred to the configuration at time t .

This kinematic description implies the following hy-

† Note that the superscript t on a variable denotes the configuration at time t in the incremental solution, and does not imply a dynamic analysis.

potheses: the director vectors remain straight during the deformations; the 'thickness' of the element measured along the director vectors remains constant during the deformations; hence only small strain conditions are considered.

Using the assumptions in (13) and (14) the geometric and material non-linear response is analysed using an incremental formulation², in which the configuration is sought for time (load step) $t + \Delta t$, when the configuration for time t is known. The basis of this incremental formulation is the use of the virtual work principle applied to the configuration at time $t + \Delta t$. In essence, two approaches can be employed leading to the updated Lagrangian and the total Lagrangian formulations. These approaches are, from a continuum mechanics point of view, equivalent, and in the following we develop the governing finite element relations for the total Lagrangian formulation.

The principle of virtual work applied to the configuration at time $t + \Delta t$ is:

$$\int_{\mathcal{V}} {}^{t+\Delta t} \tilde{S}^{ij} \delta {}^{t+\Delta t} \tilde{\epsilon}_{ij} {}^0 dV = {}^{t+\Delta t} \mathcal{R} \quad (15)$$

where the ${}^{t+\Delta t} \tilde{S}^{ij}$ are the contravariant components of the second Piola-Kirchhoff stress tensor at time $t + \Delta t$ and referred to the configuration at time 0, and the ${}^{t+\Delta t} \tilde{\epsilon}_{ij}$ are the covariant components of the Green-Lagrange strain tensor at time $t + \Delta t$ and referred to time 0. Both sets of tensor components are measured in the convected coordinate system r_i , $i=1,2,3$. The external virtual work is given by ${}^{t+\Delta t} \mathcal{R}$ and includes the work due to the applied surface tractions and body forces.

For the incremental solution, the stresses and strains are decomposed into the known quantities, ${}^t \tilde{S}^{ij}$ and ${}^t \tilde{\epsilon}_{ij}$, and unknown increments, ${}_0 \tilde{S}^{ij}$ and ${}_0 \tilde{\epsilon}_{ij}$, so that

$${}^{t+\Delta t} \tilde{S}^{ij} = {}^t \tilde{S}^{ij} + {}_0 \tilde{S}^{ij} \quad (16)$$

$${}^{t+\Delta t} \tilde{\epsilon}_{ij} = {}^t \tilde{\epsilon}_{ij} + {}_0 \tilde{\epsilon}_{ij} \quad (17)$$

In addition, the strain increment can be written as a linear part, ${}_0 \tilde{\epsilon}_{ij}$, and a non-linear part, ${}_0 \tilde{\eta}_{ij}$, hence

$${}_0 \tilde{\epsilon}_{ij} = {}_0 \tilde{\epsilon}_{ij} + {}_0 \tilde{\eta}_{ij} \quad (18)$$

Substituting from (16) to (18) into (15) and using the linearized expressions ${}_0 \tilde{S}^{ij} = {}_0 \tilde{C}^{ijkl} {}_0 \tilde{\epsilon}_{kl}$ and $\delta {}_0 \tilde{\epsilon}_{ij} = \delta {}_0 \tilde{\epsilon}_{ij}$ we obtain the linearized equation of motion:

$$\int_{\mathcal{V}} {}_0 \tilde{C}^{ijkl} {}_0 \tilde{\epsilon}_{kl} \delta {}_0 \tilde{\epsilon}_{ij} {}^0 dV + \int_{\mathcal{V}} {}^t \tilde{S}^{ij} \delta {}_0 \tilde{\eta}_{ij} {}^0 dV = {}^{t+\Delta t} \mathcal{R} - \int_{\mathcal{V}} {}^t \tilde{S}^{ij} \delta {}^t \tilde{\epsilon}_{ij} {}^0 dV \quad (19)$$

This equation is the basic equilibrium relation employed to develop the governing finite element matrices. For the actual solution of problems it is frequently important to use equilibrium iterations, but the finite element matrices and vectors used in these iterations can be derived directly from the matrices obtained using (19)². Note that ${}_0 \tilde{C}^{ijkl}$ is now obtained using (9) with the condition ${}^t \tilde{S}^{33} = 0$, which implies the more natural condition ${}^t \tilde{\epsilon}^{33} = 0$ only in the small strain case.

The basic problem of the finite element discretization of (19) lies in expressing the strain terms of (19) in terms of the finite element interpolations. Using the definition of the Green-Lagrange strain components:

$${}^t \tilde{\epsilon}_{ij} = \frac{1}{2} ({}^t g_i \cdot {}^t g_j - {}^0 g_i \cdot {}^0 g_j) \quad (20)$$

and the relations in (13) and (14) we obtain:

$${}_0 \tilde{\epsilon}_{ii} = h_{k,i} {}^t g_i \cdot \mathbf{u}_k + \frac{r_3}{2} a_k h_{k,i} (-\alpha_k {}^t g_i \cdot {}^t V_2^k + \beta_k {}^t g_i \cdot {}^t V_1^k) \quad (21a)$$

$${}_0 \tilde{\eta}_{ii} = \frac{1}{2} h_{k,i} h_{p,i} \mathbf{u}_k \cdot \mathbf{u}_p + \frac{r_3}{2} h_{k,i} h_{p,i} a_p (-\alpha_p {}^t V_2^p \cdot \mathbf{u}_k + \beta_p {}^t V_1^p \cdot \mathbf{u}_k) + \frac{(r_3)^2}{8} h_{k,i} h_{p,i} a_k a_p (-\alpha_k {}^t V_2^k + \beta_k {}^t V_1^k) \cdot (-\alpha_p {}^t V_2^p + \beta_p {}^t V_1^p) \quad (i=1,2) \quad (21b)$$

with the notation $h_{k,i} = \frac{\partial h_k}{\partial r_i}$, $\mathbf{u}_k^T = [u_1^k \quad u_2^k \quad u_3^k]$, and

$${}_0 \tilde{\epsilon}_{12} = \frac{1}{2} [h_{k,2} {}^t g_1 \cdot \mathbf{u}_k + h_{k,1} {}^t g_2 \cdot \mathbf{u}_k + \frac{r_3}{2} h_{k,2} a_k (-\alpha_k {}^t V_2^k \cdot {}^t g_1 + \beta_k {}^t V_1^k \cdot {}^t g_1) + \frac{r_3}{2} h_{k,1} a_k (-\alpha_k {}^t V_2^k \cdot {}^t g_2 + \beta_k {}^t V_1^k \cdot {}^t g_2)] \quad (22a)$$

$${}_0 \tilde{\eta}_{12} = \frac{1}{2} [h_{k,1} h_{p,2} \mathbf{u}_k \cdot \mathbf{u}_p + \frac{r_3}{2} h_{k,1} h_{p,2} a_p (-\alpha_p {}^t V_2^p \cdot \mathbf{u}_k + \beta_p {}^t V_1^p \cdot \mathbf{u}_k) + \frac{r_3}{2} h_{k,1} h_{p,2} a_k (-\alpha_k {}^t V_2^k \cdot \mathbf{u}_p + \beta_k {}^t V_1^k \cdot \mathbf{u}_p) + \frac{(r_3)^2}{4} h_{k,1} h_{p,2} a_k a_p (-\alpha_k {}^t V_2^k + \beta_k {}^t V_1^k) \cdot (-\alpha_p {}^t V_2^p + \beta_p {}^t V_1^p)] \quad (22b)$$

Further, we obtain for the transverse shear strains, using (3) and (6):

$${}_0 \tilde{\epsilon}_{13} = \frac{1}{8} (1+r_2) [{}^t g_{3i}^A (u_i^1 - u_i^2) + \frac{1}{2} {}^t g_{1i}^A (-\alpha_1 a_1 {}^t V_{2i}^1 + \beta_1 a_1 {}^t V_{1i}^1 - \alpha_2 a_2 {}^t V_{2i}^2 + \beta_2 a_2 {}^t V_{1i}^2)] + \frac{1}{8} (1-r_2) [{}^t g_{3i}^C (u_i^4 - u_i^3) + \frac{1}{2} {}^t g_{1i}^C (-\alpha_4 a_4 {}^t V_{2i}^4 + \beta_4 a_4 {}^t V_{1i}^4 - \alpha_3 a_3 {}^t V_{2i}^3 + \beta_3 a_3 {}^t V_{1i}^3)] \quad (23a)$$

$${}_0 \tilde{\eta}_{13} = \frac{1}{32} (1+r_2) [(-\alpha_1 a_1 {}^t V_{2i}^1 + \beta_1 a_1 {}^t V_{1i}^1 - \alpha_2 a_2 {}^t V_{2i}^2 + \beta_2 a_2 {}^t V_{1i}^2) (u_i^1 - u_i^2)] + \frac{1}{32} (1-r_2) [(-\alpha_4 a_4 {}^t V_{2i}^4 + \beta_4 a_4 {}^t V_{1i}^4 - \alpha_3 a_3 {}^t V_{2i}^3 + \beta_3 a_3 {}^t V_{1i}^3) (u_i^4 - u_i^3)] \quad (23b)$$

and

$${}_0 \tilde{\epsilon}_{23} = \frac{1}{8} (1+r_1) [{}^t g_{3i}^D (u_i^1 - u_i^4) + \frac{1}{2} {}^t g_{2i}^D (-\alpha_1 a_1 {}^t V_{2i}^1 + \beta_1 a_1 {}^t V_{1i}^1 - \alpha_4 a_4 {}^t V_{2i}^4 + \beta_4 a_4 {}^t V_{1i}^4)] + \frac{1}{8} (1-r_1) [{}^t g_{3i}^B (u_i^2 - u_i^3) + \frac{1}{2} {}^t g_{2i}^B (-\alpha_2 a_2 {}^t V_{2i}^2 + \beta_2 a_2 {}^t V_{1i}^2 - \alpha_3 a_3 {}^t V_{2i}^3 + \beta_3 a_3 {}^t V_{1i}^3)] \quad (24a)$$

$$\begin{aligned} \delta \tilde{\epsilon}_{23} = & \frac{1}{32}(1+r_1)[(-\alpha_1 a_1 {}^t V_{2i}^1 + \beta_1 a_1 {}^t V_{1i}^1 - \\ & \alpha_4 a_4 {}^t V_{2i}^4 + \beta_4 a_4 {}^t V_{1i}^4)(u_i^1 - u_i^4)] + \\ & \frac{1}{32}(1-r_1)[(-\alpha_2 a_2 {}^t V_{2i}^2 + \beta_2 a_2 {}^t V_{1i}^2 - \\ & \alpha_3 a_3 {}^t V_{2i}^3 + \beta_3 a_3 {}^t V_{1i}^3)(u_i^2 - u_i^3)] \end{aligned} \quad (24b)$$

Note that, since we assume the thickness of the shell to be constant, the strain ${}^t_0 \tilde{\epsilon}_{33}$ through the element thickness is zero.

The expressions in (21) to (24) are substituted into (19) which in the standard manner yields the linear strain incremental stiffness matrix ${}^t_0 \mathbf{K}_L$, the non-linear strain (or geometric) incremental stiffness matrix ${}^t_0 \mathbf{K}_{NL}$ and the nodal point force vector ${}^t_0 \mathbf{F}$ in the finite element incremental equilibrium relations²,

$$({}^t_0 \mathbf{K}_L + {}^t_0 \mathbf{K}_{NL})\mathbf{u} = {}^{t+\Delta t} \mathbf{R} - {}^t_0 \mathbf{F} \quad (25)$$

The element matrices in (25) correspond to five degrees of freedom per node (see Figure 1) but in some applications it is convenient to use instead of α_k and β_k three rotations about the global coordinate axes (see examples). In this case, we simply transform the matrices of (25) in the standard manner².

NUMERICAL TESTS AND EXAMPLE SOLUTIONS

We have implemented our shell element in the ADINA computer program and have performed various numerical tests to study the predictive capabilities of the element. The following solutions were all obtained using 2 x 2 Gauss integration in the $r_3 = 0$ surface of the element, and 2 and 4 point Gauss integration in the r_3 direction, for elastic and elastoplastic analyses, respectively.

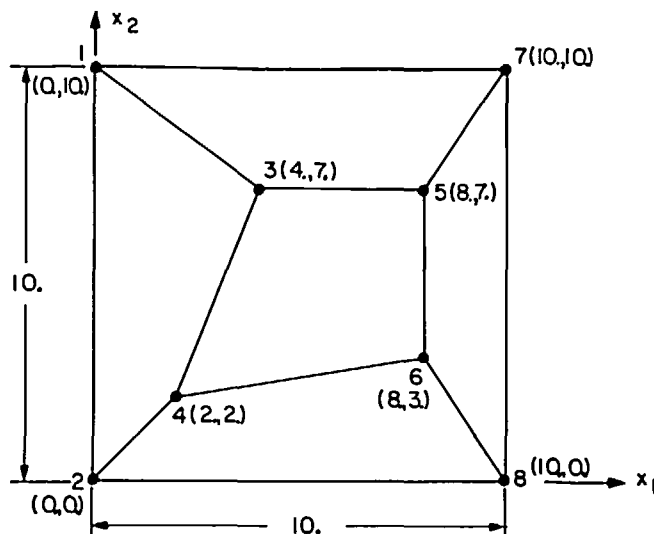
Some simple tests

As a first step to test the element, the eigenvalues of the stiffness matrices of undistorted and distorted elements were calculated. In all cases, as expected, the element displayed the six rigid body modes and no spurious zero energy modes.

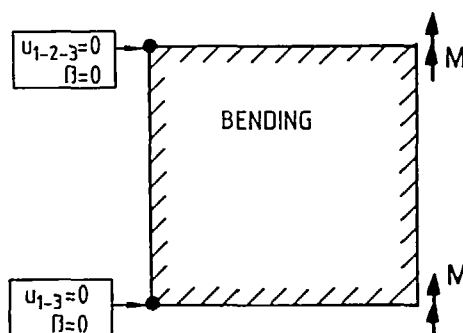
Patch tests. For the patch test^{2,18} the mesh shown in Figure 4a was used. In the first analysis (Figure 4b) the mesh was loaded with the constant moment indicated and a constant curvature (linear distribution of rotations) was obtained for both plate thicknesses in the two plate directions. The transverse displacements predicted by the model were, as expected, those of Kirchhoff-Love plate theory at nodes 7 and 8.

In the second analysis (Figure 4c) the rotational degrees of freedom were deleted and the mesh was subjected to shear forces. As expected, for both plate thicknesses a linear distribution of transverse displacements was obtained.

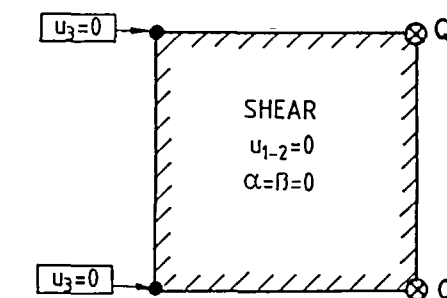
In the third analysis (Figure 4d) the mesh was subjected to an external twisting moment. In the thin plate analysis, constant curvatures were obtained in both plate directions and the transverse displacements agreed with the analytical thin plate theory solution. In the thick plate analysis, a slight non-symmetry in the displacement response (the third digit) was obtained due to the unsymmetric representation of the transverse shear deformations. This non-symmetry is not observed, if the shear deformations are suppressed (which corresponds to thin



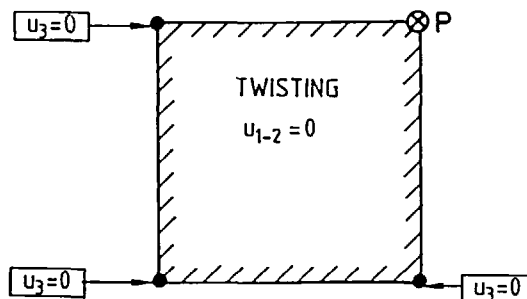
(a) Patch test mesh



(b) Constant curvature patch test

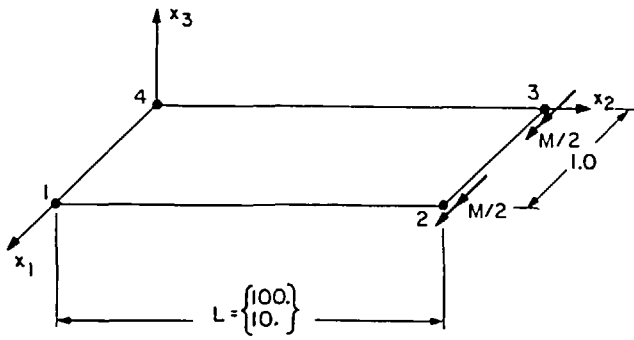


(c) Constant shear patch test (zero rotations)

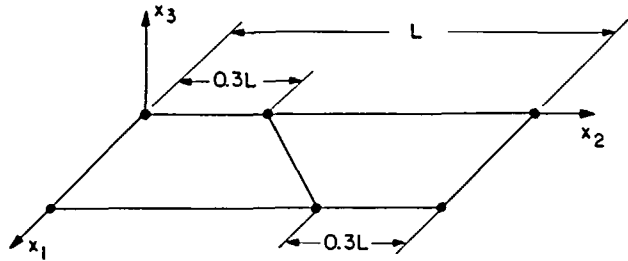


(d) Constant twist patch test

Figure 4 Patch tests. $E = 2.1 \times 10^6$; $\nu = 0.3$; thickness = $\begin{cases} 1.0 \\ 0.001 \end{cases}$



(a) One element case. Node 1: $x=0$; $u_{2-3}=0$. Node 4: $x=L$; $u_{1-2-3}=0$



(b) Two element case

Figure 5 Cantilever subjected to tip bending moment. $E=2.1 \times 10^6$; $\nu=0.3$; thickness=0.1.

plate theory) by choosing a large value for the shear correction factor k (or when using rectangular elements in the mesh)².

Finally, it should be noted that the patch test is of course passed for the three membrane stress states (τ_{11} , τ_{22} and τ_{12} constants).

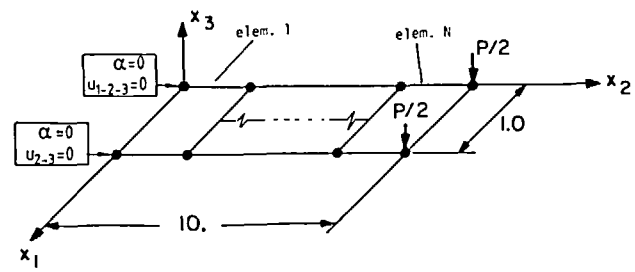
Cantilever linear analyses. A cantilever of unit width, thickness 0.1 and lengths 10 and 100 was subjected to a tip bending moment. The structure was modelled using one single element and two distorted elements as shown in Figure 5. The results obtained in these analyses for the displacements and rotations at the cantilever tip and the stresses were those of Bernoulli beam theory.

Next, the cantilever in Figure 6a was analysed for the transverse tip load shown. Using 4 equal size elements to idealize the cantilever, again good results were obtained when compared with beam theoretical results (see Figure 6b and Table 1).

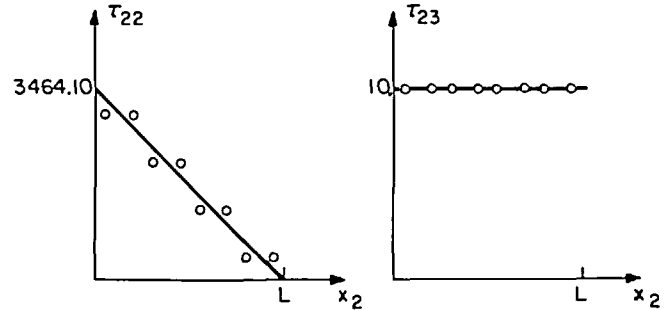
Finally, the elements modelling the cantilever were distorted as shown in Figure 6c for a thin and a thick cantilever. The results given in Figure 6d and Table 2 show that the transverse displacements and normal bending stresses are almost insensitive to the element distortions. However, the calculated transverse shear stresses (not shown in the Figure) are not accurate.

Linear analyses of a simply-supported plate. A simply-supported plate was considered for a static and a frequency analysis using a consistent mass matrix. To model one quarter of the plate the 4×4 mesh of equal elements (Figure 7a) was used. Figure 7b and Tables 3 and 4 give a comparison of the numerically and analytically predicted results. The same plate was also analysed using the distorted element mesh also shown in Figure 7a and the results of Figure 7b and Tables 3 and 4 were obtained.

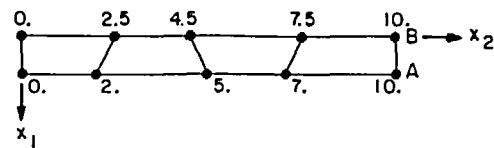
$E=2.1 \times 10^6$; $\nu=0.0$; thickness=0.1; $P=1.0$



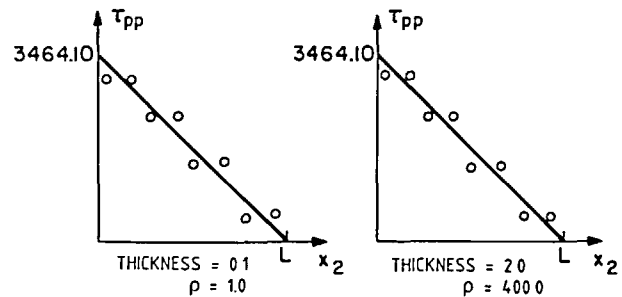
(a) Cantilever subjected to transverse tip load



(b) Solution using non-distorted elements



(c) Distorted mesh - plan view



(d) Solution using distorted mesh - two thicknesses and loads

Figure 6 Response of a cantilever subjected to transverse tip load, stresses shown are those at the Gauss integration stations $r_3=0.57735$; τ_{pp} is the principal stress in the distorted mesh, and its direction was always less than 11 degrees from the x_2 axis. —, Analytical (Bernoulli); \circ , shell element ($N=4$)

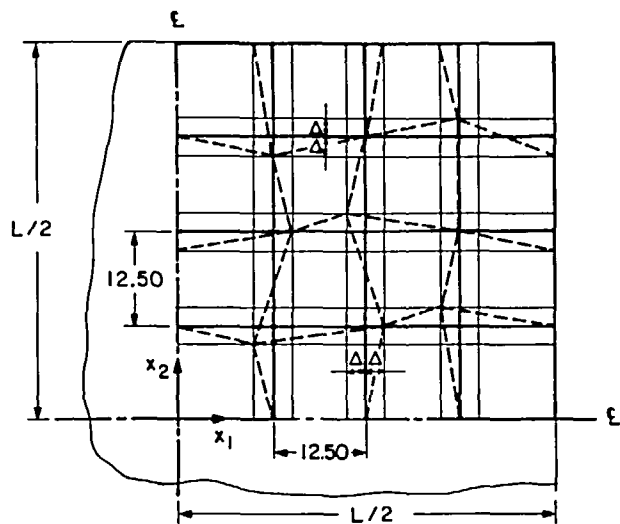
Table 1 Cantilever tip transverse displacement: non-distorted meshes of N elements

N	$u_{3TIP}^{FEM} / \left(\frac{PL^3}{3EI} + \frac{PL}{AG} \right)$
1	0.750
4	0.984

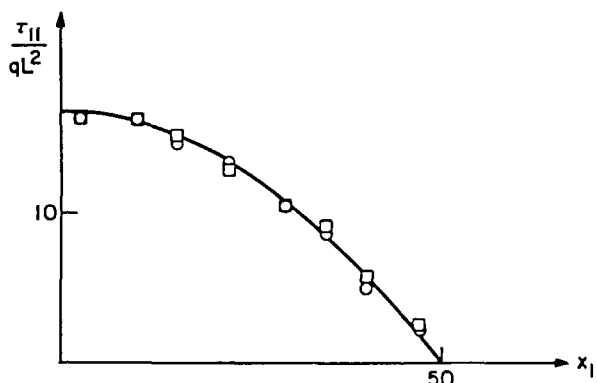
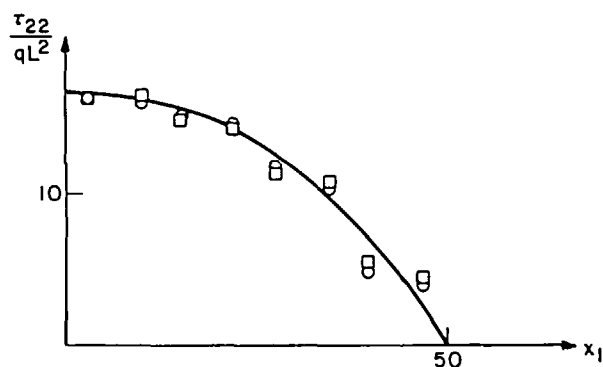
Table 2 Cantilever tip transverse displacements

Thickness	$\eta _{point B}$	$\eta _{point A}$
0.1	0.989	0.996
2.0	1.0013	0.995

$\eta = (u_3 \text{ distorted mesh}) / (u_3 \text{ non-distorted mesh})$



(a) Non-distorted and distorted meshes ($\Delta=2.50$)



(b) Static response due to constant pressure loading, stresses are given along line $x_2=0, x_3=0.028868$. —, analytical (Kirchhoff plate); ○, non-distorted mesh; □, distorted mesh.

Figure 7 Linear analysis of a simply-supported plate

Table 3 Non-dimensional displacements at centre of simply-supported plate: distorted and non-distorted meshes

Model	$u_3^{FEM}/u_3^{thin\ plate}$ at centre
non-dist.	0.995
dist.	0.992

Table 4 Non-dimensional frequencies f (cycles/sec) for a simply-supported plate: distorted and non-distorted meshes

Mode shape	$f^{FEM}/f^{thin\ plate}$
1-1	1.02
1-3	1.18
3-3	1.17

Analysis of a rhombic cantilever. The rhombic cantilever shown in Figure 8, fixed at one side and subjected to constant pressure was analysed using a 4×4 element mesh. In Table 5, the results for the transverse displacements at six locations are compared against the solutions obtained using the DKT triangular element⁶, experimental measurements¹ and using the 16-node isoparametric element (with $4 \times 4 \times 2$ Gauss integration). In all cases a one step geometric non-linear analysis with equilibrium iterations was performed. Good correspondence between the experimental results and the solution obtained using our new 4-node element is observed.

Linear analysis of a cylindrical (Scordelis-Lo) shell

The shell structure shown in Figure 9a has frequently been used to test the performance of shell elements¹². Figure 9b shows the solutions obtained with our elements. In each of the solutions uniform meshes with equal sized elements were employed over one-quarter of the shell. Solutions obtained using the 3-node DKT triangular element²⁵ and the 16-node isoparametric element²⁵ are also shown.

Linear analysis of a pinched cylinder

The pinched cylinder problem shown in Figure 10a was also frequently analysed to test shell elements. Figure 10b and Tables 6 and 7 show the convergence behaviour obtained with our new element, when comparing the finite element solutions^{11,21}. Note that using the isoparametric shell element³ also a fairly large number of degrees of freedom are required to predict the response of the cylinder accurately.

Large deflection analysis of a cantilever

The cantilever shown in Figure 11a was analysed for its large displacement and large rotation response. This is a typical problem considered to test the geometric non-linear behaviour of beam and shell elements²⁵. Figure 11a also shows the models used in the analysis.

The first two models are single element, cubic and parabolic isoparametric degenerate shell element models. Model I predicts the response of the cantilever very accurately, whereas model II yields an accurate response solution in linear analysis but locks once the element is curved in the non-linear response solution. This observation is in accordance with the results reported elsewhere⁵.

The same nodal point layouts were next employed for models III and IV using our new 4-node shell element. Figures 11b-11d give the results obtained with these models. It is seen that model III yields an accurate large displacement response prediction, and even model IV yields quite accurate results up to about 60 degrees of rotation. The computer time required in these analyses were only little different using models I, III and IV.

Another important result is shown in Table 8. As reported earlier⁵, the cubic shell element is sensitive to 'in-plane' distortions, and hence it is interesting to study the effect of using a distorted element mesh in the analysis of the cantilever (see Figures 12a and 12b). Table 8 summarizes the results obtained using the one cubic element and three 4-node elements with a nodal layout that corresponds to distorting the elements. It is seen that the predictive capability of our new 4-node element is considerably less sensitive to the element distortions.

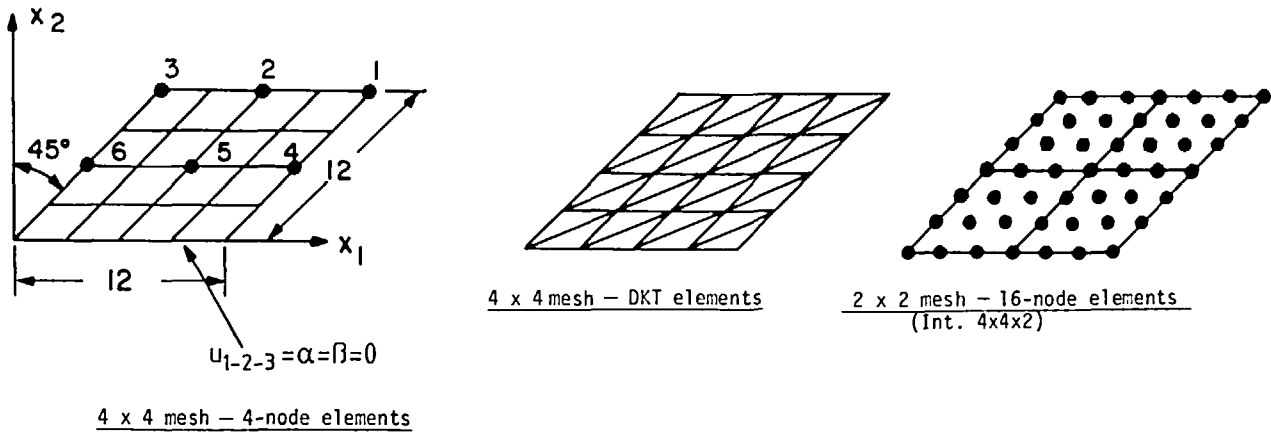


Figure 8 Response of rhombic cantilever subjected to constant pressure. $q=0.26066$; $E=10.5 \times 10^6$; thickness=0.125; $\nu=0.3$

Table 5

Element	Mesh	CPU time CPU time of DKT	Deflection at location					
			1	2	3	4	5	6
DKT	4x4	1.00	0.293	0.196	0.114	0.118	0.055	0.024
4-node	4x4	approx. 2	0.272	0.183	0.106	0.102	0.046	0.019
16-node	2x2	approx. 6½	0.266	0.182	0.110	0.105	0.048	0.019
Experimental ¹			0.297	0.204	0.121	0.129	0.056	0.022

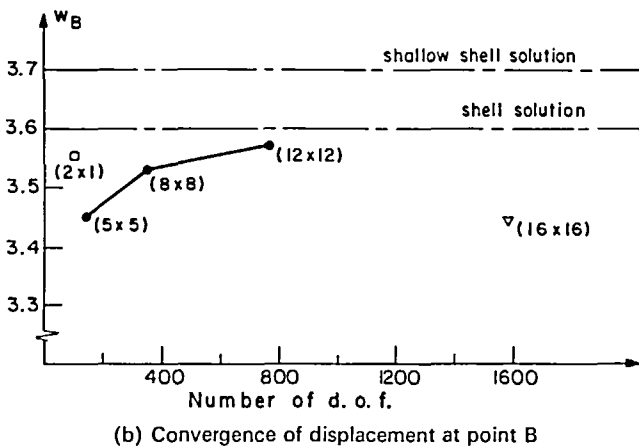
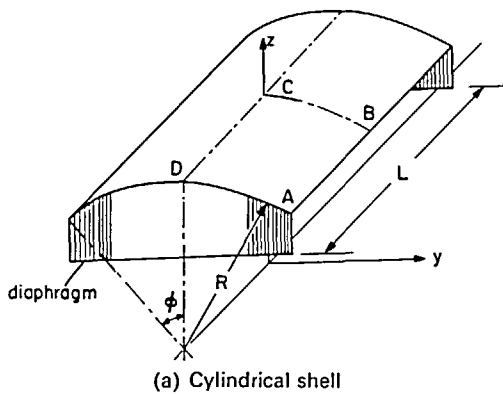


Figure 9 Linear analysis of a cylinder shell subjected to dead weight. The 2x1 result refers to the solution obtained with two 16-node shell elements spanning from C to B. The 16x16 result refers to the use of 512 equal triangular DKT elements. $R=300$; $L=600$; $\phi=40^\circ$; thickness=3.0; $E=3 \times 10^6$; $\nu=0.0$; specific weight=0.208333, ———, reference solutions; ●—●, present study; □, 16-node element (Int. 4x4x2); ▽, DKT element

Geometric non-linear response of a shallow spherical shell

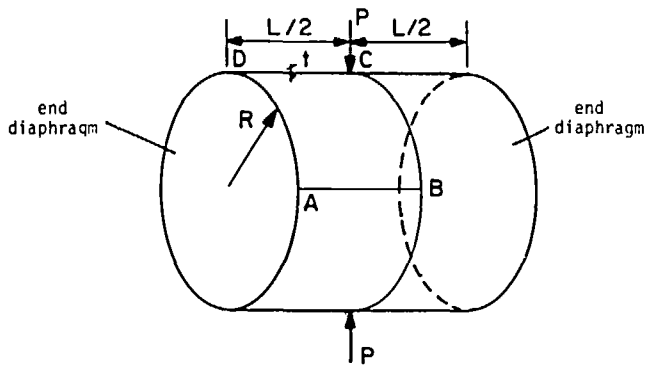
Figure 13a shows the spherical shell that was also analysed³ with one cubic shell element, modelling one-quarter of the shell. To test our new 4-node shell element, the same nodal point layout was used³, giving a mesh of nine elements. Figure 13b shows the response calculated, including the post-buckling response (not reported in ref. 3) with the automatic load stepping algorithm⁴. Good correspondence with the analytical solution of Leicester²⁰ and the solution of Horrigmo¹⁶ was obtained. The solution with the 16-node element was almost twice as expensive as the 4-node element solution (using in both cases the same parameters for the automatic step-by-step solution algorithm).

Linear buckling analysis and large deflection response of a simply-supported stiffened plate

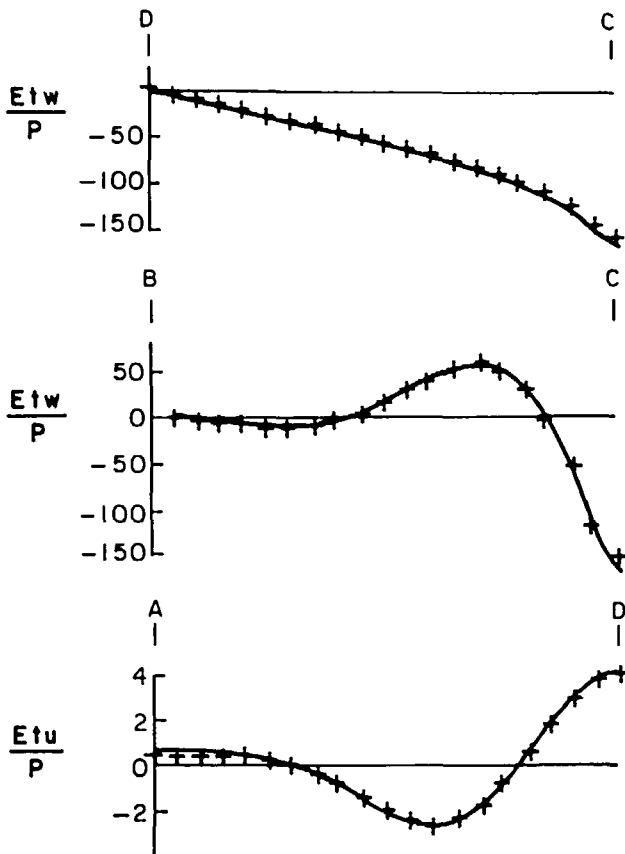
The stiffened plate shown in Figure 14a was analysed for its buckling response. Since we expect the buckling mode to be symmetric²⁶ only one-quarter of the plate is modelled using symmetry boundary conditions. The model consists of nine 4-node shell elements and three 2-node isoparametric beam elements. At the nodes where a shell element connects to a beam element, three rotational degrees of freedom aligned with the global axes are considered for the shell element. In order to avoid locking of the isoparametric beam elements, one point Gauss integration along the beam axes was used. This does not introduce spurious zero energy modes in the model although the bending stiffness of the beam is underestimated.

The linearized buckling problem was solved as described in reference 4(37) and we obtained:

$$\frac{\sigma_{cr}(\text{finite element solution})}{\sigma_{cr}(\text{analytical solution})} = 1.02$$



(a) Pinched cylinder. $R/t=100$, $L/R=2$



(b) Displacements: —, analytical solution; +, present study (20×20 mesh).

Figure 10 Linear analysis of a pinched cylinder; u =axial displacement, w =radial displacement

Table 6 Convergence study for 4-node element: pinched cylinder

Mesh for $\frac{1}{8}$ th of shell	Number of d.o.f.	$\hat{w}_C^{FEM}/\hat{w}_C^{analyt}$
5×5	130	0.51
10×10	510	0.83
20×20	2020	0.96

$$\hat{w}_C \text{ (series solution)} = -164.24 \text{ by Lindberg } et \text{ al. } \hat{w}_C = \frac{w_C Et}{P}$$

Table 7 Comparison between displacements for 4-node and 16-node elements: pinched cylinder

Element	Mesh for $\frac{1}{8}$ th of shell	Number of d.o.f.	$\hat{w}_C^{FEM}/\hat{w}_C^{analyt}$
4-node	20×20	2020	0.96
16-node	10×10	4530	0.98

Next, an initial imperfection with the shape of the first buckling mode and a maximum amplitude of 1/5 of the plate thickness was introduced. Figure 14b shows the large deflection response of this model as calculated using the automatic load stepping scheme of reference 4 with a tight energy convergence tolerance.

Analysis of elastoplastic response of a circular plate

The thin circular plate shown in Figure 15a was analysed for its elastoplastic response, when subjected to a concentrated load at its centre. The plate is simply-supported with its edges restrained from moving in its plane.

In a first solution, the plate model shown in Figure 15a was used to analyse the plate assuming small displacements (materially-non-linear-only conditions). Figure 15c shows that the theoretical collapse load is overestimated, but for the coarse mesh used, the predicted response is quite reasonable.

In a second solution, large displacements and elastoplastic conditions were assumed and in this case the stiffening behaviour of the plate shown in Figure 15c was predicted. In order to have a comparison, also the model of five axisymmetric 8-node elements shown in Figure 15b was solved. Figure 15c shows that both models predict in essence the same response; however, in this case relatively little plasticity was developed for the range of displacements considered.

CONCLUSIONS

A new four-node non-flat general non-linear shell element has been presented with the following important element properties: (1) the element is formulated using three-dimensional continuum mechanics theory; hence the use of the element is not restricted by application of a specific shell theory; (2) the element is reliable and has good predictive capability in the analysis of thick and thin shells; (3) the amount of computations required to calculate the element stiffness matrix are very closely those that are used in standard isoparametric formulations. The computer time used could be reduced considerably in elastic analysis by using analytical integration through the element thickness.

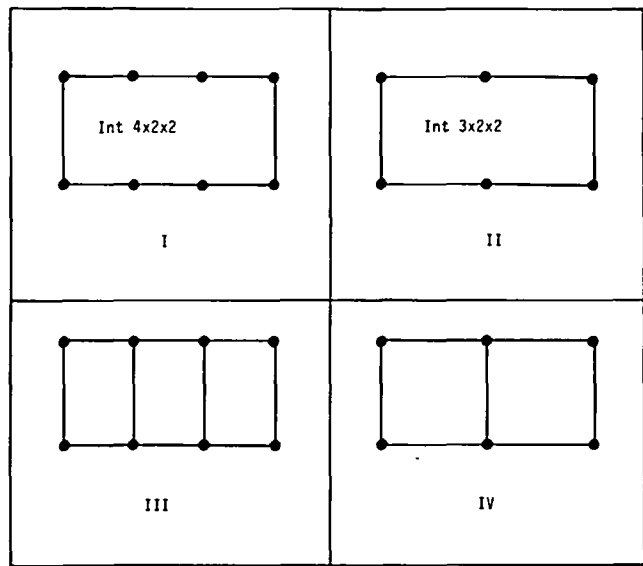
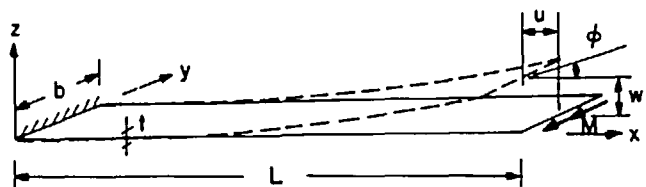
In this paper we have presented the formulation and some applications of the element. The solution results obtained are most encouraging, but a formal mathematical convergence study of the element would be very valuable, and we are currently pursuing such research.

Finally, it should be noted that the element presented here provides a very attractive basic formulation that could be extended to large strain analysis and analysis of composite shells. Also, the concepts applied here to formulate a 4-node element could equally well be employed in an effective manner to formulate higher-order shell elements.

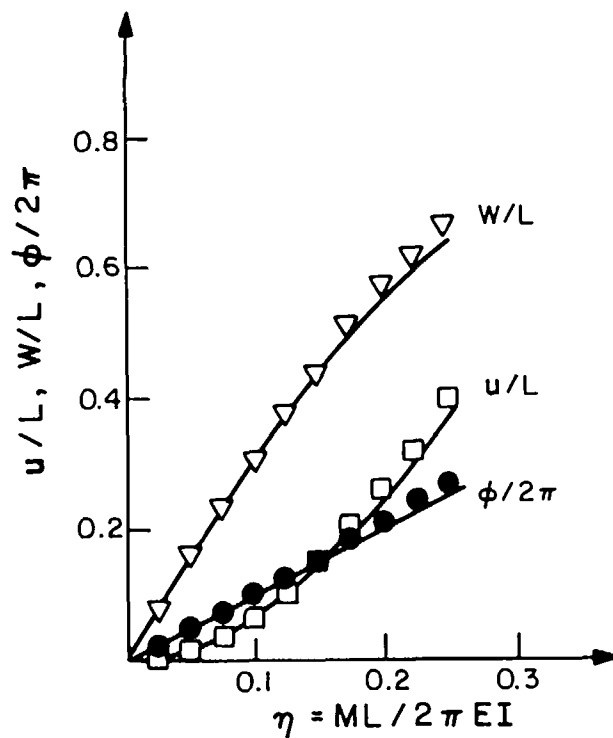
ACKNOWLEDGEMENTS

We are grateful for the financial support by the U.S. Army contract no. DAAK11-82-K-0005 and the ADINA users group for this work.

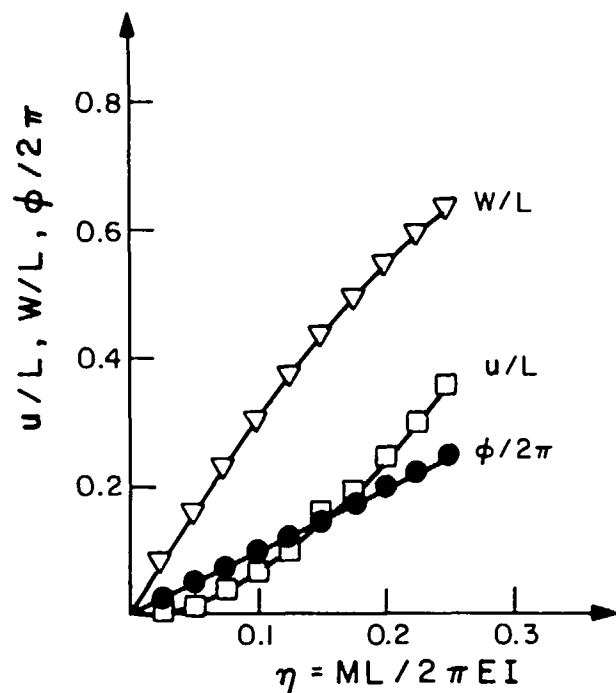
Note added in proof. — We have just learned — and regret not to have known of it earlier — that R. H. MacNeal [J. Nucl. Eng. Design, 70, 3–12 (1982)] proposed a plate element for linear analysis that is very close to the element presented above.



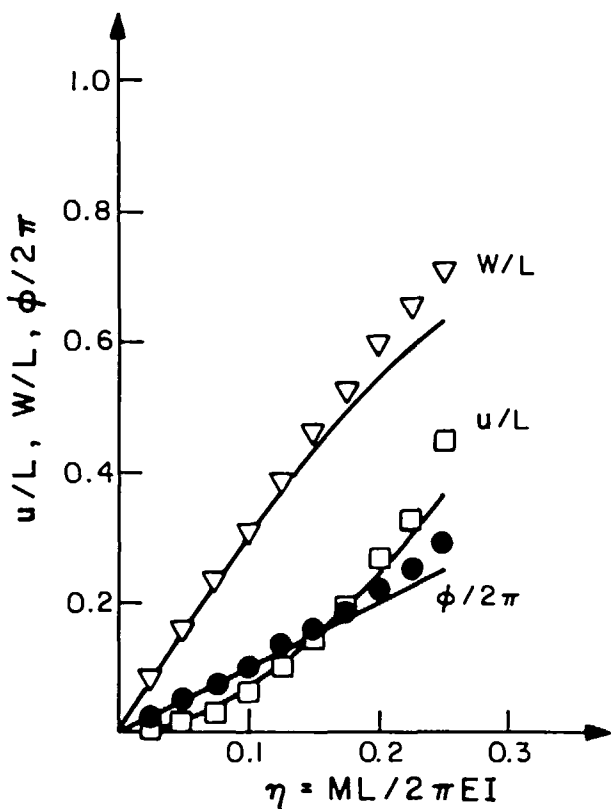
(a) Finite element models: $b=1.0$; $t=1.0$; $L=12.0$; $E=1800$; $\nu=0.0$



(c) Response of model III



(b) Response of model I

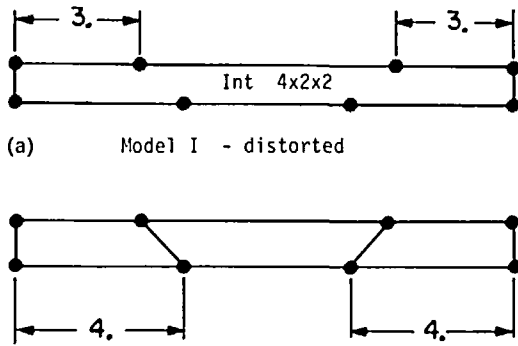


(d) Response of model IV

Figure 11 Large deflection analysis of a cantilever using non-distorted elements. —, Analytical solution, ●, □, ▽, respective model response

REFERENCES

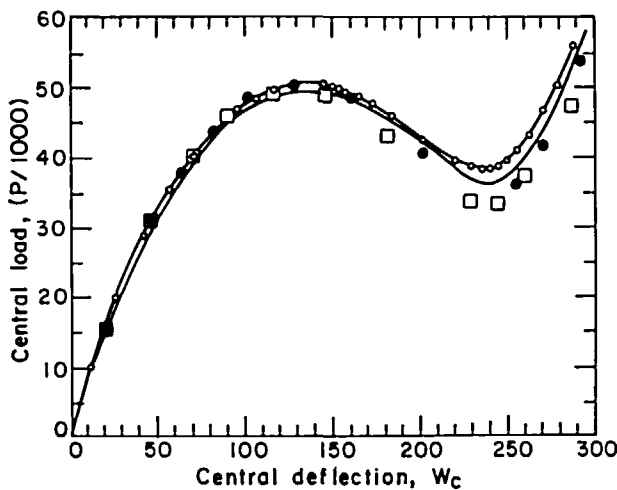
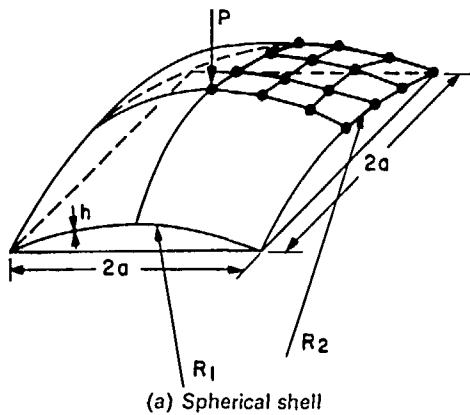
- 1 Adini, A. Analysis of shell structures by the finite element method, *PhD Dissertation*, Department of Civil Engineering, University of California, Berkeley (1961)
- 2 Bathe, K. J. *Finite Element Procedures in Engineering Analysis*, Prentice-Hall, Englewood Cliffs, New Jersey (1982)
- 3 Bathe, K. J. and Bolourchi, S. A geometric and material nonlinear plate and shell element, *J. Comput. Struct.*, 11, 23-48 (1979)
- 4 Bathe, K. J. and Dvorkin, E. N. On the automatic solution of nonlinear finite element equations, *J. Comput. Struct.* 17, (5-6), 871-879 (1983)
- 5 Bathe, K. J., Dvorkin, E. N. and Ho, L. W. Our discrete-Kirchhoff and isoparametric shell elements for nonlinear analysis - an assessment, *J. Comput. Struct.*, 16, (1-4), 89-98 (1983)



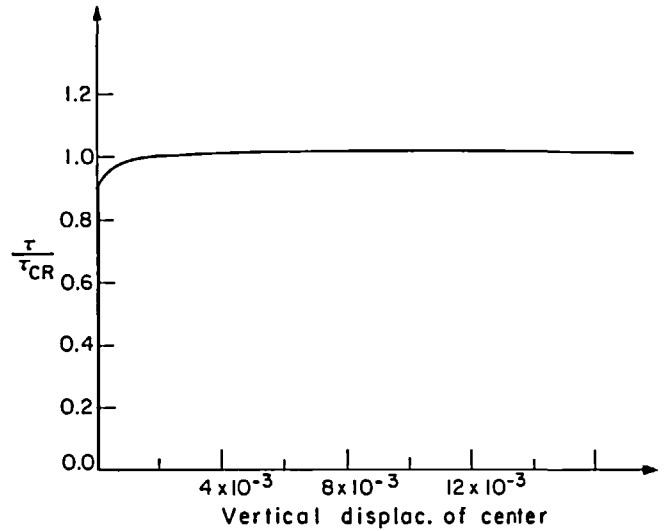
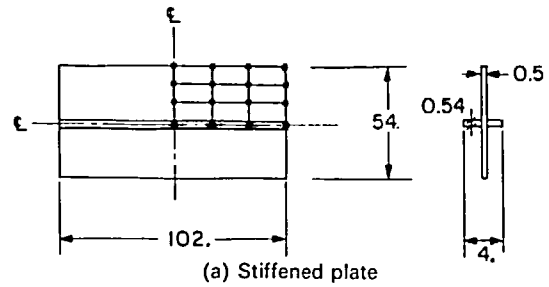
(a) Model I - distorted
(b) Model III - distorted
Figure 12 Large deflection analysis of a cantilever using distorted elements

Table 8 Results for large deflection analysis of a cantilever using distorted elements

	Model I (distorted)			Model III (distorted)		
	step 2	step 5	step 8	step 2	step 5	step 8
$\phi^{FEM} / \phi^{analyt}$	0.13	0.13	0.13	0.95	0.84	0.76
u^{FEM} / u^{analyt}	0.01	0.01	0.01	0.89	0.68	0.56
w^{FEM} / w^{analyt}	0.10	0.11	0.12	0.95	0.86	0.81
ϕ^{analyt}	18°	45°	72°	18°	45°	72°

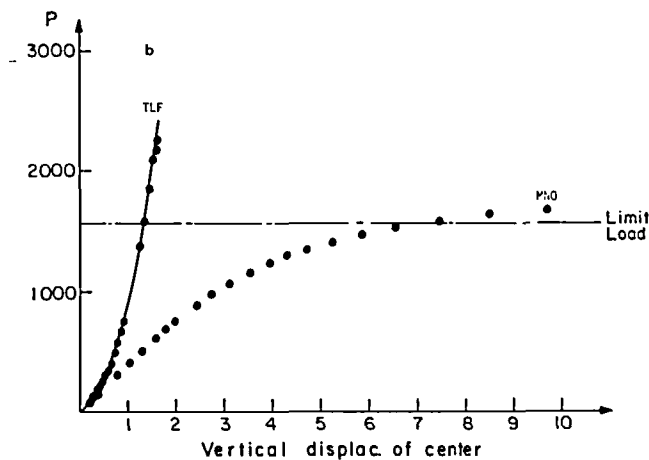
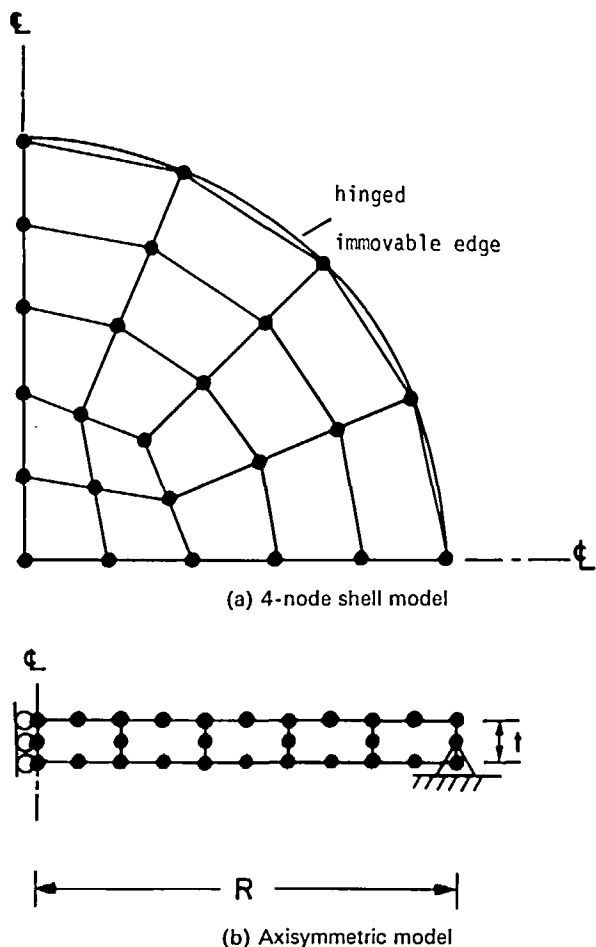


(a) Spherical shell
(b) Non-linear load displacement curve.
Figure 13 Geometric non-linear response of a spherical shell. O, Horrignoe; —, Leicester; ●, nine 4-node elements; □, one 16-node element Int 4×4×2



(a) Stiffened plate
(b) Large deflection response
Figure 14 Non-linear response of a stiffened plate. $E=2.1 \times 10^6$; $\nu=0.3$

- Bathe, K. J. and Ho, L. W. A simple and effective element for analysis of general shell structures, *J. Comput. Struct.*, **13**, 673-682 (1980)
- Bathe, K. J. and Hö, L. W. Some results in the analysis of thin shell structures, *Nonlinear Finite Element Analysis in Structural Mechanics*, (Ed. W. Wunderlich et al.), Springer-Verlag, Berlin (1981)
- Batoz, J. L., Bathe, K. J. and Ho, L. W. A study of three-node triangular plate bending elements, *Int. J. Num. Meth. Eng.*, **15**, 1771-1812 (1980)
- Batoz, J. L. and Ben Tahar, M. Evaluation of a new quadrilateral plate bending element, *Int. J. Num. Meth. Eng.*, **18**, 1655-1677 (1982)
- Bercovier, M., Hasbani, Y., Gilon, Y. and Bathe, K. J. On a finite element procedure for nonlinear incompressible elasticity, *Hybrid and Mixed Finite Element Methods*, (Ed. S. M. Atluri et al.), John Wiley, New York (1983)
- Flügge, W. *Stresses in Shells*, 2nd edn, Springer-Verlag, Berlin (1973)
- Forsberg, K. and Hartung, R. An evaluation of finite difference and finite element techniques for analysis of general shells, *Symp. High Speed Computing of Elastic Structures*, IUTAM, Liège (1970)
- Fung, Y. C. *Foundations of Solid Mechanics*, Prentice-Hall, Englewood Cliffs, New Jersey (1965)
- Gallagher, R. H. Problems and progress in thin shell finite element analysis, *Finite Elements in Thin Shells and Curved Members*, (Ed. D. G. Ashwell and R. H. Gallagher), John Wiley, New York (1976)
- Green, A. E. and Zerna, W. *Theoretical Elasticity*, 2nd edn, Oxford University Press (1968)
- Horrignoe, G. Finite element instability analysis of free-form shells, *Report 77-2*, Division of Structural Mechanics, The Norwegian Institute of Technology, University of Trondheim, Norway (1977)
- Hughes, T. J. R. and Liu, W. K. Nonlinear finite element analysis of shells: Part I, Three-dimensional shells, *J. Comput. Meth. Appl. Mech. Eng.*, **26**, 331-362 (1981)



(c) Elastoplastic load-displacement curve

Figure 15 Response of elastic-perfectly plastic circular plate subjected to a concentrated load, P , at its centre. TLF abbreviates use of total Lagrangian formulation and MNO abbreviates use of materially non-linear-only formulation. $R=100$, $t=1$; $E=2.1 \times 10^6$; $E_T=0.0$; $\nu=0.3$; $\sigma_y=1000$. Circular plate response; —, axisymmetric model; ●, 4-node shell model

18 Irons, B. M. and Razzaque, A. Experience with the patch test for convergence of finite elements. *The Mathematical Foundations of the Finite Element Method with Applications to Partial Differential Equations*, (Ed. A. K. Aziz, Academic Press, New York (1972)

19 Kråkeland, B. Nonlinear analysis of shells using degenerate isoparametric elements, *Finite Elements in Nonlinear Mechanics*, Vol. 1, (Ed. P. G. Bergan *et al.*), Tapir Publishers (Norwegian Institute of Technology, Trondheim, Norway) (1978)

20 Leicester, R. H. Finite deformations of shallow shells, *Proc. Am. Soc. Civil Eng.*, **94**, (EM6), 1409-1423 (1968)

21 Lindberg, G. M., Olson, M. D. and Cowper, G. R. New developments in the finite element analysis of shells, *Q. Bull. Div. Mech. Eng. and the National Aeronautical Establishment*, National Research Council of Canada, Vol. 4 (1969)

22 MacNeal, R. H. A simple quadrilateral shell element, *J. Comput. Struct.*, **8**, 175-183 (1978)

23 Noor, A. K. and Peters, J. M. Mixed models and reduced/selec-

tive integration displacement models for nonlinear analysis of curved beams, *Int. J. Num. Meth. Eng.*, **17**, 615-631 (1981)

24 Ramm, E. and Sattelle, J. M. Elasto-plastic large deformation shell analysis using degenerated elements, *Nonlinear Finite Element Analysis of Plates and Shells*, (Ed. T. J. R. Hughes), AMD-Vol. 48, Am. Soc. Mech. Eng., New York (1981)

25 Report AE 83-5, ADINA System Verification Manual, ADINA Engineering, Västerås, Sweden and Watertown, Mass. (1983)

26 Timoshenko, S. P. and Gere, J. M. *Theory of Elastic Stability*, 2nd edn, McGraw-Hill, New York (1961)

27 Washizu, K. *Variational Methods in Elasticity and Plasticity*, Pergamon Press, Oxford and New York (1968)

28 Wempner, G., Talaslidis, D. and Hwang, C.-M. A simple and efficient approximation of shells via finite quadrilateral elements, *J. Appl. Mech.*, **49**, 115-120 (1982)

29 Zienkiewicz, O. C. *The Finite Element Method*, McGraw-Hill, New York (1977)